Choroidal Neovascularization Analyzed on Ultrahigh-Speed Swept-Source Optical Coherence Tomography Angiography Compared to Spectral-Domain Optical Coherence Tomography Angiography

Citation: Novais, Eduardo A.; Adhi, Mehreen; Moult, Eric M. et al. "Choroidal Neovascularization Analyzed on Ultrahigh-Speed Swept-Source Optical Coherence Tomography Angiography Compared to Spectral-Domain Optical Coherence Tomography Angiography." American Journal of Ophthalmology 164 (April 2016): 80–88 © 2016 Elsevier Inc

As Published: http://dx.doi.org/10.1016/j.ajo.2016.01.011

Publisher: Elsevier

Persistent URL: http://hdl.handle.net/1721.1/110907

Version: Author's final manuscript: final author's manuscript post peer review, without publisher's formatting or copy editing

HHS Public Access

Author manuscript

Am J Ophthalmol. Author manuscript; available in PMC 2017 April 01.

Published in final edited form as:

Am J Ophthalmol. 2016 April ; 164: 80–88. doi:10.1016/j.ajo.2016.01.011.

Choroidal neovascularization analyzed on ultra-high speed swept source optical coherence tomography angiography compared to spectral domain optical coherence tomography angiography

Eduardo A. Novais[1,2], **Mehreen Adhi**[1,3], **Eric M. Moult**[3], **Ricardo N. Louzada**[1,4], **Emily D. Cole**[1,3], **Lennart Husvogt**[3,5], **ByungKun Lee**[3], **Sabin Dang**[1], **Caio V. S. Regatieri**[1,2], **André J. Witkin**[1], **Caroline R. Baumal**[1], **Joachim Hornegger**[5,6], **Vijaysekhar Jayaraman**[7], **James G Fujimoto**[3], **Jay S. Duker**[1], and **Nadia K. Waheed**[1,*]

[1]New England Eye Center, Tufts Medical Center, Boston, Massachusetts

[2]Federal University of São Paulo, School of Medicine, São Paulo, Brazil

[3]Department of Electrical Engineering and Computer Science, Research Laboratory of Electronics, Massachusetts Institute of Technology, Cambridge, MA

[4]Federal University of Goiás, Goiânia, Brazil

[5]Pattern Recognition Lab., Friedrich-Alexander University Erlangen-Nürnberg (FAU), Erlangen, Germany

[6]Erlangen Graduate School in Advanced Optical Technologies (SAOT), Erlangen, Germany

[7]Praevium Research Inc., Santa Barbara, California

Abstract

Purpose—To compare visualization of choroidal neovascularization (CNV) secondary to age-related macular degeneration (AMD) using an ultra-high speed swept-source (SS)-optical coherence tomography angiography (OCTA) prototype versus a spectral-domain (SD)-OCTA device.

Design—Comparative analysis of diagnostic instruments.

[*]**Corresponding Author/Reprint Requests:** Nadia K Waheed, MD, MPH, New England Eye Center at Tufts Medical Center, 260 Tremont Street, Biewend Building, 9 – 11th Floor, Boston, MA 02116, T: 617-636-7950, F: 617-636-4866, nadiakwaheed@gmail.com.

DISCLOSURE:

Conflicts of Interest: Jay S. Duker is a consultant for and receives research support from Carl Zeiss Meditec, OptoVue, and Topcon Medical Systems Inc.; and has stock in Hemera Biosciences Inc., EyeNetra, and Ophthotech Corp. Nadia K. Waheed was a consultant for Iconic therapeutics, served the speaker's bureau for Thrombogenics, and received research support from Carl Zeiss Meditec, Inc. Caroline Baumal received a travel grant from Optovue and served on an advisory board for Allergan. James G. Fujimoto: Royalties from intellectual property owned by the Massachusetts Institute of Technology and licensed to Carl Zeiss Meditec Inc., Optovue Inc.; Stock options – Optovue Inc. V. Jayaraman – Stock and employment at Praevium Inc., Royalties from Thorlabs Inc. There are no conflicting relationships for any other author.

Methods—Patients were prospectively recruited to be imaged on SD-OCT and SS-OCT devices on the same day. The SD-OCT device employed is the RTVue Avanti that operates at ~840nm wavelength and 70,000 A-scans/second. The SS-OCT device used is an ultra-high speed long-wavelength prototype that operates at ~1050nm wavelength and 400,000 A-scans/second. Two observers independently measured the CNV area on OCTA *en face* images from the two devices using ImageJ. The non-parametric Wilcoxon signed-rank test was used to compare area measurements and *p*-values of <0.05 were considered statistically significant.

Results—Fourteen eyes from 13 patients were enrolled. The CNV in 11 eyes (78.6%) were classified as type-1, 2 eyes (14.3%) as type-2, and 1 eye (7.1%) as mixed type. Total CNV area measured using SS-OCT and SD-OCT 3mm × 3mm OCTA were 0.949 ± 1.168mm^2 and 0.340 ± 0.301mm^2, respectively (*p=0.001*). For the 6mm × 6mm OCTA the total CNV area using SS-OCT and SD-OCT were 1.218 ± 1.284mm^2 and 0.604 ± 0.597mm^2, respectively (*p=0.0019*). The field of view did not significantly affect the measured CNV area (*p=0.19* and *p=0.18* for SS-OCT and SD-OCT respectively).

Conclusion—SS-OCTA yielded significantly larger CNV areas than SD-OCTA. It is possible that SS-OCTA is better able to demarcate the full extent of CNV vasculature.

Introduction

Fluorescein angiography (FA) and indocyanine green angiography (ICGA) are considered the gold standard for imaging the retinal and choroidal vasculature, and in particular, for imaging choroidal neovascularization.[1–3] These imaging modalities are dynamic and visualize dye transit over time, allowing direct visualization of large vessel filling and eventual leakage and/or pooling of dye. However, small retinal vessels and feeder vessels are often obscured by subsequent hyperfluorescence, especially in the late phase of dye transit, and may limit precise assessment of the extent of neovascularization. In addition, these modalities are invasive involving the use of intravenous contrast that can result in systemic side effects and rarely anaphylaxis.[4–6]

Optical coherence tomography angiography (OCTA) is a non-invasive technology that uses the decorrelation motion contrast between rapidly repeated Optical coherence tomography (OCT) B-scans to visualize blood flow.[7–9] Recently, spectral-domain (SD) OCTA systems were introduced using prototype software on a commercially available device operating at a ~840 nm wavelength. Using spectral-domain OCTA, evaluation of choroid neovascularization (CNV) in eyes with wet age-related macular degeneration (AMD) has been described.[7,10,11] However, since these systems operated at short wavelengths, visualization beneath the retinal pigment epithelium (RPE) may be obscured due to signal attenuation from the RPE-Bruch's membrane complex.[12,13]

Swept-source (SS-OCT) technology uses a longer, ~1050 nm wavelength and has less variation in sensitivity with depth (sensitivity roll off) compared with SD-OCT, allowing improved immunity to ocular opacity and deeper penetration into the choroid.[14,15] This allows an improved visualization of the choroid both on cross-sectional as well as *en face* OCTA imaging,[16,17] and may also improve visualization of CNV, especially the sub-RPE component of the membrane. As OCTA imaging becomes more ubiquitous, a comparison

between these two imaging paradigms—SD-OCT and SS-OCT—becomes increasingly important. The present study aimed to utilize an ultra-high speed SS-OCT prototype to analyze the extent of CNV and quantify its area in eyes with wet AMD when compared to SD-OCT.

Methods

This was a comparative analysis of diagnostic instruments conducted at the New England Eye Center of Tufts Medical Center (Boston, Massachusetts) and approved by the Tufts Medical Center and Massachusetts Institute of Technology Institutional Review Boards. The research adhered to the tenets of the Declaration of Helsinki and complied with the Health Insurance Portability and Accountability Act of 1996. Written informed consent was obtained before OCTA imaging.

Patient Selection

Patients with CNV secondary to AMD were seen at the Retina service of New England Eye Center between August 2014 and May 2015 and prospectively recruited to be imaged on SD-OCT and SS-OCT. To be included, a comprehensive chart review was performed to confirm the diagnosis of CNV secondary to wet AMD that was made by a retina specialist on the basis of a complete ophthalmic evaluation including dilated fundus examination, standard structural SD-OCT imaging and FA and/or ICGA.

Image Acquisition and Analysis

All patients were imaged on SD-OCT and SS-OCT on the same day. The SD-OCT instrument was the RTVue Avanti with prototype AngioVue® software for OCTA (Optovue, Inc., Fremont, CA). This instrument operates at ~840 nm wavelength and 70,000 A-scans per second to acquire OCTA volumes consisting of 2 repeated B-scans from 304 sequentially uniformly spaced locations. Each B-scan consisted of 304 A-scans for a total of 2 × 304 × 304 A-scans per acquisition, with a total acquisition time of approximately 3 seconds, and an axial optical resolution of ~5μm. Split-spectrum amplitude-decorrelation angiography (SSADA) was employed to improve the signal-to-noise ratio.[18,19] Motion correction was performed using registration of 2 orthogonally acquired volumes.[20,21] The SS-OCT device was an ultra-high speed ~1050 nm prototype developed at Massachusetts Institute of Technology (Cambridge, Massachusetts) and deployed to New England Eye Center. It uses a high speed vertical cavity surface emitting laser as the light source and operates at a ~1050 nm wavelength achieving a speed of 400,000 A-scans per second, and acquires a total of 5 repeated B-scans from 500 sequentially uniformly spaced locations. Each B-scan consisted of 500 A-scans, and the interscan time was approximately 1.5 msec (accounting for the galvanometer mirror scanning duty cycle). A total of 5 × 500 × 500 A-scans were acquired per OCTA volume with an acquisition time of approximately 3.8 seconds, and an axial optical resolution of ~8–9μm. For both 3 mm × 3 mm and 6 mm × 6 mm, the acquired OCT volumes were centered on the fovea. There was no eye tracking used for fixation in the SS-OCT. The patients were asked to fixate on an internal target during OCTA acquisition. The motion correction algorithm on the SS-OCT prototype is similar to the SD-OCT system and consists of acquiring OCTA volumes in orthogonal X-fast and Y-

fast directions. From these two orthogonal scans a single merged volume is constructed that has superior signal quality and reduced motion artifacts.[20]

Two independent and masked readers (EAN and RNL) of the Boston Image Reading Center analyzed the 3 mm × 3 mm and 6 mm × 6 mm OCTA images from both devices to determine the extent of CNV. For the SD-OCT images, they used the automatic segmentation of the retinal layers at the level of the choriocapillaris generated by the AngioVue software in an orthogonal view. In order to correct for automated segmentation error and projection artifacts which can obscure the full extent of the CNV, the segmentation slab was manually adjusted, using corresponding structural OCT B-scans as a guide for the placement of two parallel segmentation lines at sequential depths, so as to best visualize the CNV complex. This semi-automatic method allowed the readers to select images that visualized the largest extent of the CNV for subsequent quantitative analysis. For the SS-OCT images, a custom C++ application was used for processing, and Image J (National Institutes of Health, Bethesda, Maryland, USA) was used for visualization. A flat segmentation line was manually adjusted using the orthogonal view, and *en face* OCTA images were computed by projecting the OCTA data through the depths spanned by the lesion.

Two observers independently measured the area of CNV on OCTA images from the two instruments using Image J. Both 3 mm × 3 mm and 6 mm × 6 mm OCTA images were quantitatively analyzed. The pixel dimensions of the original images were used to set the scale using Image J plugins prior to performing the measurements. The measurements were rescaled to the millimeter square unit using pixel dimensions of the OCTA images.

Data statistical analysis

Statistical analysis was performed with Stata 14 (StataCorp. 2015. *Stata Statistical Software: Revision 23*. College Station, TX: StataCorp LP). Intraclass correlation coefficient (ICC) was used to estimate the agreement between individual measurements from both readers. Since the ICC was consistently > 0.9 between the two readers, the Wilcoxon Signed-rank test was used to compare area measurements performed by one reader on SD-OCT and SS-OCT 3 mm × 3 mm and 6 mm × 6 mm OCTA scans. *P*-values of <0.05 were considered statistically significant.

Results

Patient demographics

Fourteen eyes from 13 Caucasian patients were enrolled in this study. Nine patients (64.3%) were female and 5 (35.7%) were male. The mean age of the studied population was 73.5 ± 10.6 years. All patients had anti vascular endothelial growth factor (anti-VEGF) treatment prior to imaging. Patient demographics and number of intravitreous injections are listed in the Table.

Qualitative analysis

OCTA enabled detailed *en face* visualization of the neovascular complex; the corresponding structural OCT B-scans helped identify the depth and location of the CNV relative to the RPE. Features on B-scan such as the presence or absence of subretinal fluid, intraretinal fluid, subretinal hyper-reflective material and presence/absence of PED were evaluated and found to be identical between the SS and the SD-OCT images. The CNV for each patient was classified using OCTA and corresponding structural B-scans: type 1, when the CNV complex was under the RPE; type 2 when it was above the RPE; and mixed when both components were present. Of the 14 eyes from 13 patients enrolled in this study, 11 (78.6%) presented a type 1 CNV, 2 (14.3%) presented a type 2 CNV, and only one eye (7.1%) had the mixed type. CNV classifications for each patient are listed in the Table. All eyes were imaged with both devices using 3 × 3 mm and 6 × 6 mm protocols. In one eye, only 3 × 3 mm images were used, as the 6 × 6 mm images from the SD-OCT were of too poor quality for analysis.

In 26 of 27 images analyzed with 3 mm × 3 mm (14) and 6 mm × 6 mm (13) OCTA, SS-OCT visualized a larger area of the CNV complex compared to SD-OCT. This discrepancy in the extent of CNV visualized by the two devices was correlated with corresponding FA images when present. It appeared that the occult part of the CNV was the major contributor to the difference in the extent of CNV visualized by the two devices. SD-OCT at ~840 nm wavelength is unable to completely visualize the occult component of the neovascular membrane in all patients (Figure 1). Additionally, in 1 patient with type 1 (occult) CNV, SD-OCT was unable to identify the neovascular membrane whereas SS-OCT at ~1050 nm wavelength was able to clearly capture the full extent of the membrane (Figure 2). Both instruments however, were able to identify the feeder vessel (Figure 3). Using the 3 mm × 3 mm field of view, both the SD-OCT and SS-OCT instruments visualized the feeder vessel in 5 (35.7%) of the 14 eyes. Using the 6 mm × 6 mm field of view, SD-OCT and SS-OCT visualized the feeder vessels in the 5 (38.5%) and 6 (46.2%) of the 13 eyes, respectively (Figure 4).

Quantitative analysis

The mean CNV area (± SD) for SS-OCT and SD-OCT 3 mm × 3 mm OCTA images was 0.95 ± 1.17 mm^2 and 0.34 ± 0.30 mm^2, respectively (*p=0.001*). For the 6 mm × 6 mm OCTA images the total CNV areas for the SS-OCT and SD-OCT were 1.22 ± 1.28 mm^2 and 0.60 ± 0.6 mm^2, respectively (*p=0.0019*). On a sub analysis of the type 1 CNV area, the SS-OCT and SD-OCT 3 mm × 3 mm OCTA images showed areas of 1.09 ± 1.28 mm^2 and 0.36 ± 0.33 mm^2, respectively (*p=0.003*). For the 6 mm × 6 mm OCTA images the Type 1 CNV was 1.31 ± 1.43 mm^2 on the SS-OCT, and 0.67 ± 0.67 mm^2 (*p=0.005*). The field of view did not significantly affect the measured CNV area from the same eye measured using 3 mm × 3 mm OCTA versus the 6 mm × 6 mm OCTA images from the same device, although there was a trend toward larger CNV areas measured using 6×6mm OCTA images (*p=0.19* and *p=0.18* for SS-OCT and SD-OCT respectively). The ICC for the CNV area measurements between the two observers was greater than 97% (confidence interval: 0.92 to 0.99) demonstrating reproducibility and consistency of the methodology. All measurements are listed in the Table.

Discussion

OCTA is a new non-invasive imaging technology that can visualize the retinal and choroidal vasculature. This technology is increasingly being used to image CNV membranes since it can visualize the neovascular complex both above and beneath the RPE.[22] However, signal attenuation from the RPE, media opacity or retinal hemorrhage means that, it is not always possible to fully visualize CNV, especially type 1 CNV lesions.[10] This limitation has previously been reported in ~850 nm wavelength SD-OCT.[12,13] Our study suggests that *en face* OCTA images from ~1050 nm wavelength ultra-high speed SS-OCT may provide a more accurate representation of CNV lesions compared to the ~840 nm wavelength SD-OCT.

In a recent publication using the same SD-OCT instrument used in this study, de Carlo *et al* reported a specificity of 91% and a sensitivity of only 50% for detecting CNV using OCTA.[7] The low sensitivity may be due to signal attenuation resulting from hemorrhage or to the location of CNV beneath, and in close approximation to, the RPE-Bruch's membrane complex. Previous studies comparing SS-OCT and SD-OCT B-scans suggest that the increased penetration of ~1050 nm wavelengths allows for improved imaging beneath the RPE.[23–26] However, to the authors' knowledge, a direct comparison of SS-OCT and SD-OCT angiography for visualizing CNV has not been conducted to-date.

Correlating cross-sectional OCTA images with corresponding structural OCT B-scans provides additional information, since structural OCT can help identify signs of active CNV such as intraretinal and subretinal fluid.[27,28] The authors used both FA and structural OCT to determine the location of the CNV relative to the RPE/Bruch's membrane complex to classify the CNV as type 1, type 2, or mixed.

CNV area measurement difference between SD-OCT and SS-OCT was observed in all patients with type 1 CNV (Table), and this difference was statistically significant. There may be several possible explanations for this, however, in our study we believe the difference is most likely to attributable to two factors, both related to signal strength: (1) SS-OCT systems are less susceptible to sensitivity roll-off than SD-OCT systems, and (2) SS-OCT systems operate at a longer, ~1050 nm wavelength, which allows for increased penetration below the RPE. In the SD-OCT, the imaging system is most sensitive to signals coming from reflectors close to the zero-delay; as a reflector is moved away from the zero-delay, the system will become less sensitive to the back-reflected signals.[29] This sensitivity roll-off is due to the limited spectral resolution of the spectrometers that are used SD-OCT systems. In contrast, SS-OCT systems do not use spectrometer-based detection and, instead, it is the instantaneous linewidth of the swept light source, along with the analog-to-digital acquisition rate, that determines the sensitivity roll-off of the system. This difference enables SS-OCT systems to have improved sensitivity roll-off compared to SD-OCT systems.[30] The longer wavelength of the SS-OCT systems allows for increased penetration because the RPE contains melanin, whose absorption and scattering decrease with increasing wavelength.[15]

Both sensitivity roll-off and RPE attenuation result in lower signal strengths. Because lower signal strengths cause the speckle pattern to become unstable, even in regions without flow,

most OCTA systems have an intensity-based thresholding step wherein areas of low signal are masked out to avoid spurious decorrelations. This masking process can result in areas having flow but low signal being displayed as black (no flow in the resulting OCTA image. The result is low signal levels—due to sensitivity roll-off, RPE attenuation, or any other cause—can cause OCTA to be silent even if flow is present. In the context of this study, where 11 (78.57%) of the 14 eyes were classified as type 1 CNV, which lie below the RPE, reduced signal strength combined with OCTA intensity-based thresholding is a plausible explanation for the difference in visualizations when using these two systems.

The structure and fine vascular details of CNV complex patterns are more prominent in OCTA images compared to FA and ICGA, especially with respect to size, location, and presence of feeder vessels.[31] Although the 3 mm × 3 mm OCTA images visualize the detailed vascular structure of the CNV complex, the 6 mm × 6 mm OCTA images were also evaluated in this study since the neovascular membrane can extend beyond the 3 mm × 3 mm area in some cases. In this study, there was no difference in the CNV area measured on 3 mm × 3 mm and 6 mm × 6 mm angiographic scans on the same instrument, although there was a trend to larger areas measured using the 6×6mm protocol.

Both SS-OCT and SD-OCT *en face* OCTA images were able to identify the feeder vessels, which were defined by thick central trunk with vessels radiating in all directions from the center of the lesion. Since both devices utilize decorrelation signals, it was expected that the increased flow of the trunk vessel be easily identified on both devices. Jia *et al* recently published a study using SD-OCT angiography in which they investigated the capability of OCTA in imaging and quantifying CNV in neovascular AMD patients and also reported a higher CNV flow associated with larger CNV area was likely characteristic of more chronic and mature neovascular structure.[22]

Limitations of this study include a relatively small sample size. The SD-OCT segmentation software follows the curvature of the retinal structures when segmenting the *en face* OCTA. However, it requires manual adjustments to visualize the full extent of CNV. The software used to process the SS-OCT data in the present study does not have automated segmentation. Hence, manual adjustment of the segmentation boundaries was employed to achieve the best quality image showing the full extent of CNV. More robust automated segmentation and the ability to manually alter the segmentations for accuracy are important future developments in both SD-OCT and SS-OCT software. Additionally, even though SS-OCTA systems were able to better detect the full extent of the CNV, this does not, at the present time, impact the management of patients since it is the presence or absence of CNV on OCTA in conjunction with signs of activity on OCT B scans, that is used to guide treatment.

Even though FA remains the gold standard for diagnosing CNV, it is invasive and is not depth-resolved.[32] OCTA is a noninvasive and fast technique for three-dimensional and depth-resolved imaging, allowing different vascular layers of the retina and choroid to be simultaneously visualized. The appearance of the CNV using *en face* OCT images might ultimately be used to guide retreatment, augmenting current features such as intraretinal and subretinal fluid or pigment epithelial detachments that are markers in cross sectional

structural OCT images. Thus a better visualization of the extent of CNV using SS-OCT over SD-OCT may have clinical relevance since the identification of the full extent of neovascular membrane with OCTA may improve the ability to directly evaluate the response of the pathologic vessels to the anti-VEGF therapy and better assess the efficacy of the treatment.

Supplementary Material

Refer to Web version on PubMed Central for supplementary material.

Acknowledgments

Financial Support: This work was in part supported by a grant from the Macula Vision Research Foundation, New York, National Institute of Health (NIH R01-EY011289-28, R44-EY022864-03, R01-CA075289-17), Air Force Office of Scientific Research (AFOSR FA9550-10-1-0551 and FA9550-12-1-0499), Thorlabs matching funds to Praevium Research Inc and by an MVRF grant to study wet AMD. Additional support from the Massachusetts Lions Clubs, a Samsung Scholarship, and a Natural Sciences and Engineering Research Council of Canada Scholarship. EAN and RNL are researchers supported by CAPES Foundation, Ministry of Education of Brazil, Brasilia, DF, Brazil.

Biographies

Dr. Eduardo Novais performed his ophthalmology training at the State University of Rio de Janeiro (UERJ), Brazil, followed by a clinical and surgical retina fellowship at the Federal University of São Paulo (UNIFESP) / School of Medicine, Brazil between 2009 and 2015. As a member of clinical research in ophthalmology of UNIFESP, he collaborated with Professor Rubens Belfort Jr. in many clinical trials. His research interests include imaging in AMD and in diabetic retinopathy and he is currently pursuing a Ph.D. focused on diabetic retinopathy. At present, he is an OCT research fellow at New England Medical Center at Tufts University, with Dr. Jay S. Duker and Dr. Nadia K. Waheed.

Dr. Nadia K. Waheed is an Assistant Professor of Ophthalmology at the Tufts University School of Medicine in Boston. She received her medical degree *summa cum laude* from the

Aga Khan University Medical School and a Master degree from the Harvard School of Public Health. She completed a residency in Ophthalmology and a Fellowship in Retina at the Massachusetts Eye and Ear Infirmary. Her research interests include ocular imaging, diabetic eye disease and age related macular degeneration.

References

1. Kotsolis AI, Killian FA, Ladas ID, Yannuzzi LA. Fluorescein angiography and optical coherence tomography concordance for choroidal neovascularisation in multifocal choroidtis. Br J Ophthalmol. 2010; 94(11):1506–1508. [PubMed: 20472744]
2. Do DV. Detection of new-onset choroidal neovascularization. Curr Opin Ophthalmol. 2013; 24(3): 244–247. [PubMed: 23518615]
3. Stanga PE, Lim JI, Hamilton P. Indocyanine green angiography in chorioretinal diseases: indications and interpretation: an evidence-based update. Ophthalmology. 2003; 110(1):15–21. quiz 22-3. [PubMed: 12511340]
4. Ha SO, Kim DY, Sohn CH, Lim KS. Anaphylaxis caused by intravenous fluorescein: clinical characteristics and review of literature. Intern Emerg Med. 2014; 9(3):325–330. [PubMed: 24293212]
5. Musa F, Muen WJ, Hancock R, Clark D. Adverse effects of fluorescein angiography in hypertensive and elderly patients. Acta Ophthalmol Scand. 2006; 84(6):740–742. [PubMed: 17083530]
6. Garski TR, Staller BJ, Hepner G, Banka VS, Finney RA Jr. Adverse reactions after administration of indocyanine green. JAMA Ophthalmol. 1978; 240(7):635.
7. de Carlo TE, Bonini Filho MA, Chin AT, et al. Spectral-domain optical coherence tomography angiography of choroidal neovascularization. Ophthalmology. 2015; 122(6):1228–1238. [PubMed: 25795476]
8. Jonathan E, Enfield J, Leahy MJ. Correlation mapping method for generating microcirculation morphology from optical coherence tomography (OCT) intensity images. J Biophotonics. 2011; 4(9):583–587. [PubMed: 21887769]
9. An L, Wang RK. In vivo volumetric imaging of vascular perfusion within human retina and choroids with optical micro-angiography. Opt Express. 2008; 16(15):11438–11452. [PubMed: 18648464]
10. Kuehlewein L, Bansal M, Lenis TL, et al. Optical Coherence Tomography Angiography of Type 1 Neovascularization in Age-Related Macular Degeneration. Am J Ophthalmol. 2015; 160(4):739–748. [PubMed: 26164826]
11. Baumal CR, de Carlo TE, Waheed NK, Salz DA, Witkin AJ, Duker JS. Sequential Optical Coherence Tomographic Angiography for Diagnosis and Treatment of Choroidal Neovascularization in Multifocal Choroiditis. JAMA Ophthalmol. 2015; 133(9):1087–1090. [PubMed: 26111344]
12. Saito M, Iida T, Nagayama D. Cross-sectional and en face optical coherence tomographic features of polypoidal choroidal vasculopathy. Retina. 2008; 28(3):459–464. [PubMed: 18327139]
13. Ueno C, Gomi F, Sawa M, Nishida K. Correlation of indocyanine green angiography and optical coherence tomography findings after intravitreal ranibizumab for polypoidal choroidal vasculopathy. Retina. 2012; 32(10):2006–2013. [PubMed: 22772392]
14. Povazay B, Hermann B, Unterhuber A, et al. Three-dimensional optical coherence tomography at 1050 nm versus 800 nm in retinal pathologies: enhanced performance and choroidal penetration in cataract patients. J Biomed Opt. 2007; 12(4):041211. [PubMed: 17867800]
15. Unterhuber A, Povazay B, Hermann B, Sattmann H, Chavez-Pirson A, Drexler W. In vivo retinal optical coherence tomography at 1040 nm – enhanced penetration into the choroid. Opt Express. 2005; 13(9):3252–3258. [PubMed: 19495226]
16. Adhi M, Liu JJ, Qavi AH, et al. Choroidal analysis in healthy eyes using swept-source optical coherence tomography compared to spectral domain optical coherence tomography. Am J Ophthalmol. 2014; 157(6):1272–1281. [PubMed: 24561169]

17. Moult E, Choi W, Waheed NK, et al. Ultrahigh-speed swept-source OCT angiography in exudative AMD. Ophthalmic Surg Lasers Imaging Retina. 2014; 45(6):496–505. [PubMed: 25423628]
18. Jia Y, Tan O, Tokayer J, et al. Split-spectrum amplitude-decorrelation angiography with optical coherence tomography. Opt Express. 2012; 20(4):4710–4725. [PubMed: 22418228]
19. Tokayer J, Jia Y, Dhalla AH, Huang D. Blood flow velocity quantification using split-spectrum amplitude-decorrelation angiography with optical coherence tomography. Biomed Opt Express. 2013; 4(10):1909–1924. [PubMed: 24156053]
20. Kraus MF, Potsaid B, Mayer MA, et al. Motion correction in optical coherence tomography volumes on a per A-scan basis using orthogonal scan patterns. Biomed Opt Express. 2012; 3(6): 1182–1199. [PubMed: 22741067]
21. Kraus MF, Liu JJ, Schottenhamml J, et al. Quantitative 3D-OCT motion correction with tilt and illumination correction, robust similarity measure and regularization. Biomed Opt Express. 2014; 5(8):2591–2613. [PubMed: 25136488]
22. Jia Y, Bailey ST, Wilson DJ, et al. Quantitative optical coherence tomography angiography of choroidal neovascularization in age-related macular degeneration. Ophthalmology. 2014; 121(7): 1435–1444. [PubMed: 24679442]
23. Copete S, Flores-Moreno I, Montero JA, Duker JS, Ruiz-Moreno JM. Direct comparison of spectral-domain and swept-source OCT in the measurement of choroidal thickness in normal eyes. Br J Ophthalmol. 2014; 98(3):334–338. [PubMed: 24288394]
24. Matsuo Y, Sakamoto T, Yamashita T, Tomita M, Shirasawa M, Terasaki H. Comparisons of choroidal thickness of normal eyes obtained by two different spectral-domain OCT instruments and one swept-source OCT instrument. Invest Ophthalmol Vis Sci. 2013; 54(12):7630–7636. [PubMed: 24168999]
25. Ting DS, Cheung GC, Lim LS, Yeo IY. Comparison of swept source optical coherence tomography and spectral domain optical coherence tomography in polypoidal choroidal vasculopathy. Clin Experiment Ophthalmol. 2015.07.17. 10.1111/ceo.12580
26. de Bruin DM, Burnes DL, Loewenstein J, et al. In vivo three-dimensional imaging of neovascular age-related macular degeneration using optical frequency domain imaging at 1050 nm. Invest Ophthalmol Vis Sci. 2008; 49(10):4545–4552. [PubMed: 18390638]
27. Liakopoulos S, Ongchin S, Bansal A, et al. Quantitative optical coherence tomography findings in various subtypes of neovascular age-related macular degeneration. Invest Ophthalmol Vis Sci. 2008; 49(11):5048–5054. [PubMed: 18566473]
28. Giani A, Luiselli C, Esmaili DD, et al. Spectral-domain optical coherence tomography as an indicator of fluorescein angiography leakage from choroidal neovascularization. Invest Ophthalmol Vis Sci. 2011; 52(8):5579–5586. [PubMed: 21693602]
29. Imamura Y, Fujiwara T, Margolis R, Spaide RF. Enhanced depth imaging optical coherence tomography of the choroid in central serous chorioretinopathy. Retina. 2009; 29(10):1469–1473. [PubMed: 19898183]
30. Grulkowski I, Liu JJ, Potsaid B, et al. Retinal, anterior segment and full eye imaging using ultrahigh speed swept source OCT with vertical-cavity surface emitting lasers. Biomed Opt Express. 2012; 3(11):2733–2751. [PubMed: 23162712]
31. Mastropasqua R, Di Antonio L, Di Staso S, et al. Optical Coherence Tomography Angiography in Retinal Vascular Diseases and Choroidal Neovascularization. J Ophthalmol. 2015.09.27. 10.1155/2015/343515
32. Coscas G, Lupidi M, Coscas F, Francais C, Cagini C, Souied EH. Optical Coherence Tomography Angiography during Follow-Up: Qualitative and Quantitative Analysis of Mixed Type I and II Choroidal Neovascularization after Vascular Endothelial Growth Factor Trap Therapy. Ophthalmic Res. 2015; 54(2):57–63. [PubMed: 26201877]

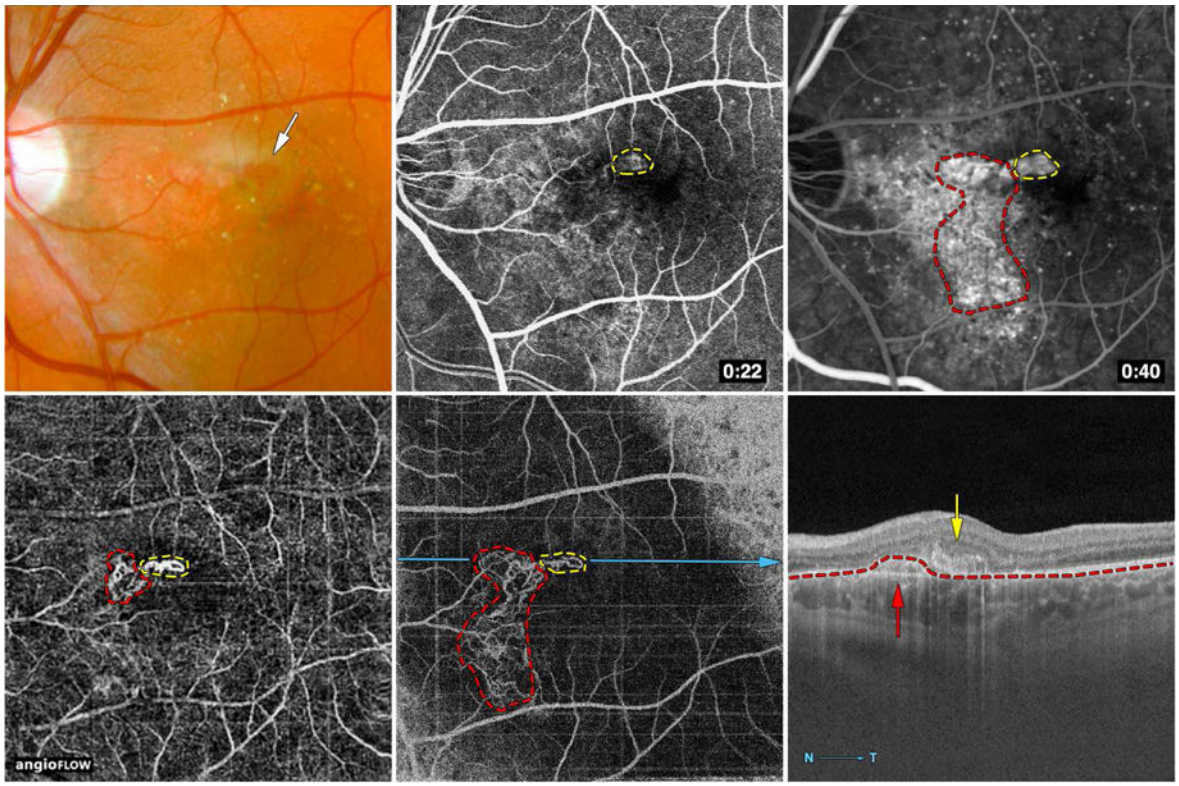

Figure 1.

Multimodal imaging of a left eye with mixed type 1 and type 2 choroidal neovascularization. (Top left) Color fundus photography. Retinal pigment epithelium (RPE) clumps and mottling, and subretinal hemorrhage (white arrow) surrounded by edematous retina and drusen.; (Top center) and (Top right) Different stages fluorescein angiography. Red dashed-line representing the occult component; yellow dashed-line representing the classic component.; (Bottom left) Spectral-domain ~840 nm wavelength optical coherence tomography angiography (OCTA) image and; (Bottom center) Swept-source ~1050 nm wavelength OCTA image. Red dashed-line representing the type 1 component; yellow dashed-line representing the type 2 component.; (Bottom right) Corresponding optical coherence tomography B-scan. RPE represented as red dashed-line. Type 1 component (red arrow) and type 2 component (yellow arrow).

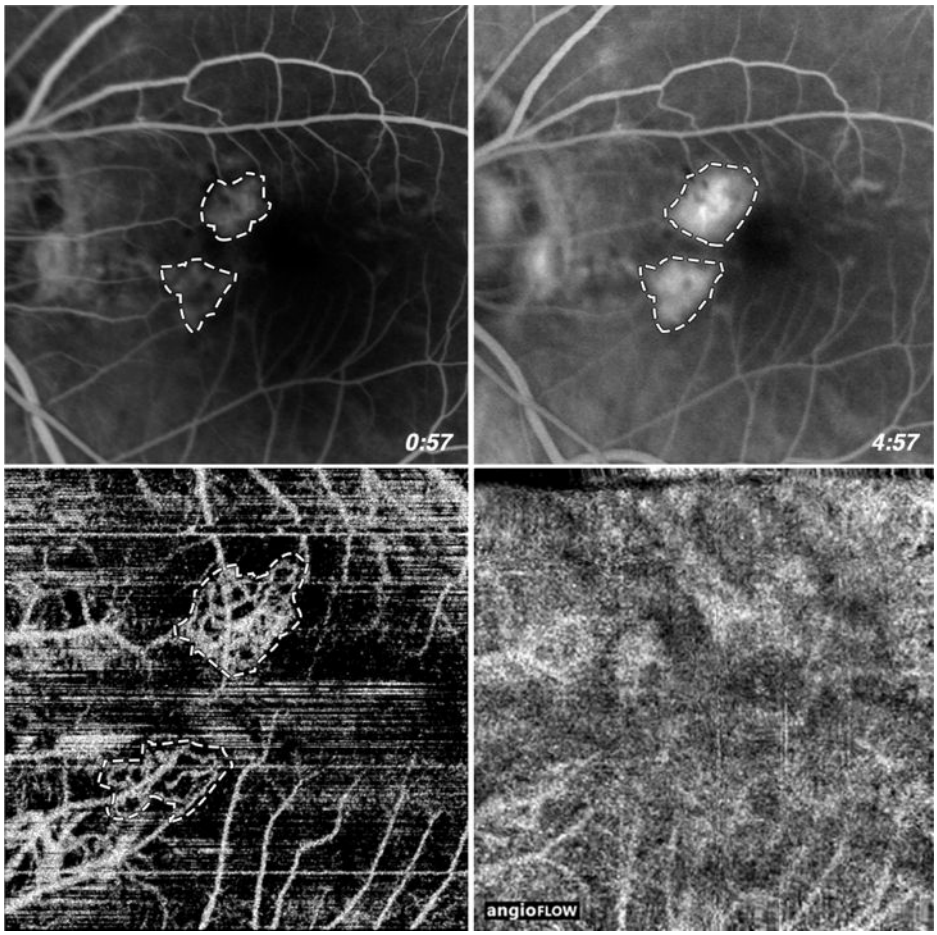

Figure 2.

Multimodal imaging of a left eye with active choroidal neovascularization (CNV). (Top left) and (Top right) Fluorescein angiography (FA). Active CNV presented as increased leakage throughout FA phases (times are shown in the lower right hand corners). (Bottom left) Swept-source optical coherence tomography angiography (OCTA) image. CNV identified (white dashed-line). (Bottom right) Spectral-domain OCTA image. No clear CNV identified.

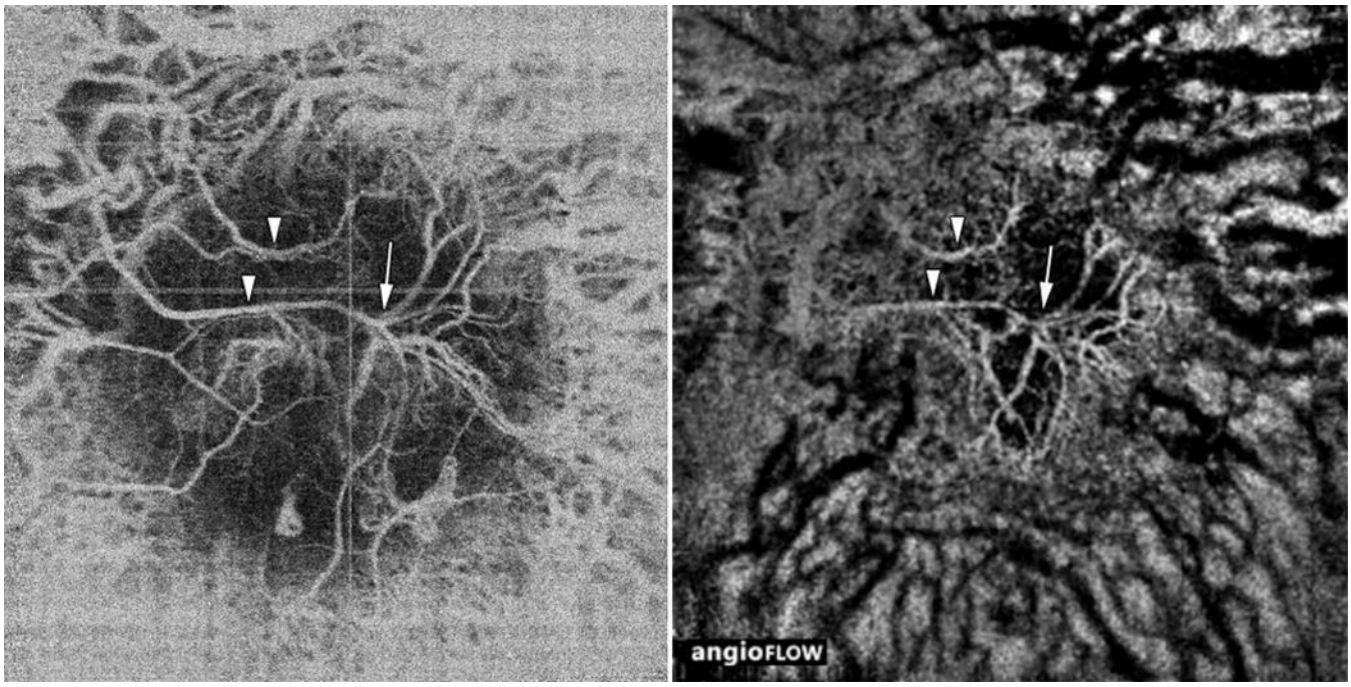

Figure 3.

Identification of feeder vessels on Swept-source (SS-) and Spectral-domain (SD-) optical coherence tomography angiography (OCTA). (Left) SS-OCTA image. (Right) SD-OCTA image. Feeder vessel (white arrowheads) and feeder trunk (white arrow).

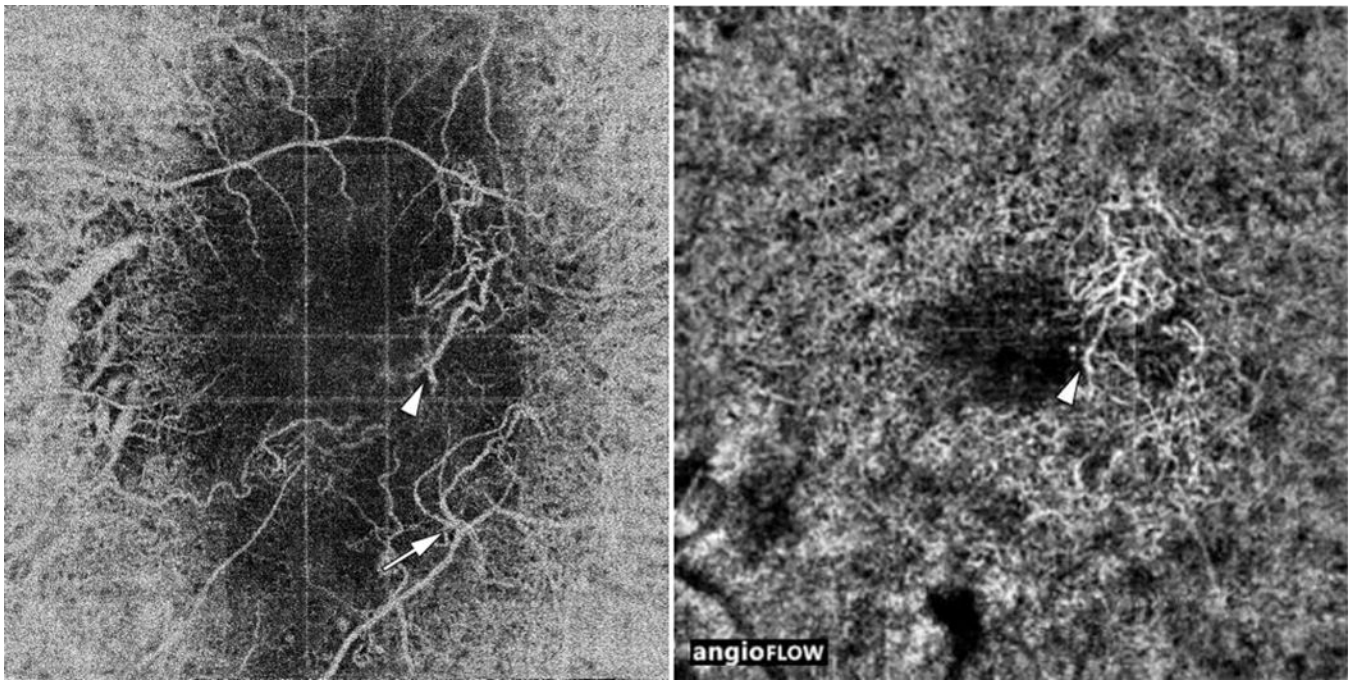

Figure 4.

Identification of feeder vessels on Swept-source (SS-) and Spectral-domain (SD-) optical coherence tomography angiography (OCTA). (Left) Swept-source OCTA image. Two feeder vessels identified (white arrowhead and white arrow). (Right) Spectral-domain OCTA image. Only one feeder vessel identified (white arrowheads.

Table

Patient demographics, choroidal neovascularization type, anti-vascular endothelial growth factor treatment profile prior imaging, and area measurements

Age	Sex	CNV type	Number of Anti- VEGF IVI	Time since last Anti-VEGF IVI (weeks)	SS-OCT 3×3 (mm^2)	SD-OCT 3×3 (mm^2)	SS-OCT 6×6 (mm^2)	SD-OCT 6×6 (mm^2)
79	F	1	35	9	4.624	0.536	Not Available	Not Available
87	F	1	3	6	1.111	0.680	4.236	1.038
56	M	2	2	8	0.787	0.519	1.492	0.519
61	F	1	11	13	0.541	0.279	0.437	0.167
66	F	1	1	4	0.632	CNV not identified	0.507	CNV not identified
81	M	1	3	4	0.405	0.371	0.368	0.355
73	F	1	17	8	0.482	0.121	0.365	0.303
57	F	Mixed	2	4	0.121	0.093	0.105	0.108
83	M	1	6	12	0.634	0.271	0.489	0.418
83	M	2	8	12	0.368	0.253	1.107	0.584
69	F	1	4	8	1.901	0.386	3.391	1.973
83	F	1	16	10	0.229	0.039	1.611	1.586
68	F	1	2	15	0.108	0.105	0.110	0.099
83	M	1	13	16	1.348	1.119	1.623	0.712

CNV = Choroid neovascularization

SS-OCT = Swept-source optical coherence tomography

SD-OCT = Spectral-domain optical coherence tomography

IVI = Intravitreous Injection

Anti-VEGF = Anti-vascular endothelial growth factor